Chapter 5
On the Calculation of the Initial Temperature Slope: Key Considerations for the Fatigue Limit Estimation

Mohammad Zaeimi, Ali Mahmoudi, Rosa De Finis, Davide Palumbo, Michael M. Khonsari, and Umberto Galietti

Abstract Over the past four decades, infrared thermography has become a popular non-destructive technique for identifying thermal signature associated with fatigue of material. In this work, by conducting experimental stepwise tests on SS316 samples and employing a unique dataset, a comparison is performed in terms of fatigue limit estimation between different thermal indices, including the mean temperature rise, slope of the mean temperature, first and second harmonic amplitudes of temperature and slope of the mean temperature in cooling stage. However, the main contribution of the work is proposing key considerations in calculating the initial slope of temperature to the purpose of better accuracy and reliability in estimating the thermal fatigue limit from temperature data. It is shown that the time interval and thermal acquisition can affect its measurements.

Keywords Thermographic method · Rapid fatigue estimation · Fatigue assessments · Thermal index · Initial slope of the temperature

Introduction

Investigating the fatigue phenomena offers crucial information for choosing effective materials because the majority of structures experience cyclic loadings throughout their life [1]. The cyclic nature of the fatigue loading creates dislocations, which in turn leads to plastic deformation. Depending on the loading level, it causes microscopic flaws [2–4] to grow and build into macroscopic cracks, and by propagation of macroscopic crack, fatigue failure happens [5].

Over the years, infrared thermography has shown to be a useful and adaptable instrument in the field of experimental mechanics. It enables thorough investigations of structural integrity [6], the defect detection in different materials (steel plates [7], composite structures [8], additively manufactured [9]) and welded joints [10], the study of fatigue cracks [11]), the stress analysis [12] and fatigue assessment [13–15].

In fatigue assessments using infrared thermography, rapid tests were initially designed in the work of La Rosa and Risitano [16] to cut down on testing time and costs. This methodology involves the application of a sequence of incremental loading blocks with constant amplitude leading the material to be subjected to various damage regimes within the loading levels [16].

Following this work, several researchers proposed distinct rapid methods for fatigue limit prediction under cyclic loading which can be categorized in three different groups [13]: (i) direct temperature assessment, (ii) thermoelastic stress analysis and (iii) energy-based approaches. The first one focuses on measuring the mean temperature increase [16] and analyzing

Mohammad Zaeimi · Davide Palumbo · Umberto Galietti
Department of Mechanics, Mathematics and Management, Polytechnic University of Bari, Via Orabona, Bari 70126, Italy
email: mohammad.zaeimi@poliba.it; davide.palumbo@poliba.it; umberto.galietti@poliba.it

Ali Mahmoudi · Michael M. Khonsari
Department of Mechanical and Industrial Engineering, Louisiana State University, 3283 Patrick Taylor Halkl, Baton Rouge, LA 70803, USA
email: alimahmoudi@lsu.edu; khonsari@lsu.edu

Rosa De Finis
University of Salento, Department of Engineering for Innovation, Piazza Tancredi, 73100, Lecce, Italy
email: rosa.definis@unisalento.it

Garrett Pataky et al. (eds.), *Fracture, Fatigue, Failure, Damage Evolution and Thermomechanics & Infrared Imaging, Vol. 4*,
Conference Proceedings of the Society for Experimental Mechanics Series, https://doi.org/10.13052/97887-438-0830-5_5

the initial slope of the temperature [17]. The second one includes the loss of adiabatic conditions through thermoelastic phase analysis [18] and the deviation from linearity in the first amplitude harmonic [19, 20]. Furthermore, the last one explores fatigue behavior through second amplitude harmonics [21], specific heat loss [22], and entropy-based methods [23]. However, the fatigue assessment using the thermographic technique was proposed to be assessed during a static test, by studying the end of the thermoelastic effect [24].

Interested readers are referred to the work by Zaeimi et al. [13] for a more comprehensive review of all thermography-based approaches for fatigue limit estimation, and the work by Colombo and Vergani [25] and Ricotta et al. [26] for comparing different thermal indices in fatigue limit estimation.

In this work, as the main contribution, the challenges associated with measuring one of the thermal indices, the initial slope of temperature, are discussed. Moreover, five thermal indices including the mean temperature rise, slope of the mean temperature, first and second harmonic amplitudes of temperature and slope of the mean temperature in cooling stage are compared using the same dataset.

Next sections are organized as follows: First, the details about the procedure and experimental setup for rapid evaluation of fatigue limit are provided. Next, the data are prepared and the results are proposed. Finally, the last section concludes the study.

Experiments

Three Stainless Steel 316 (SS 316) samples were used in stepwise tests to prepare essential data for comparing the effectiveness of various thermal indices in fatigue limit prediction. Table 1 and Figure 1 show the material characteristics and geometry of a cylindrical dog bone sample, respectively. In Table 1, ρ is the density, C_p, α and k are respectively the specific heat at constant pressure, thermal expansion and conductivity coefficients; ϵ is the emissivity factor. E, σ_y and σ_u are Young's modulus, yield strength and ultimate strength, correspondingly.

Table 1 Material properties of SS 316 [27]

$\rho\ (kg/m^3)$	$C_p\ (J/kg\ ℃)$	$k\ (W/m\ ℃)$	$\alpha\ (1/℃)$	ϵ	$E\ (GPa)$	$\sigma_y\ (MPa)$	$\sigma_u\ (MPa)$
7900	490	16.3	17.2e-6	0.98	171	335	640

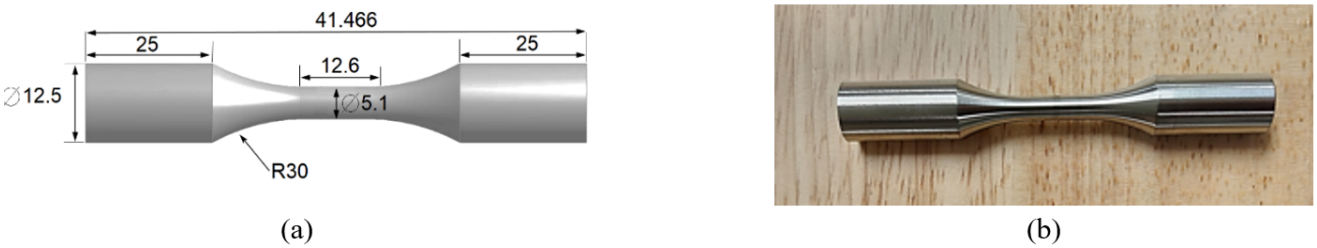

Fig. 1 (a) cylindrical dog bone geometry (in mm) and (b) fabricated sample

As shown in Table 2, a sequence of 12 incremental loading stages was used in the stepwise experiments. Every step is completed with the stress ratio $R = -1$ and a fixed loading frequency of 11 Hz. According to Table 2, the stress amplitude (σ_a) is raised until the material fails after around 20,000 cycles for each stage.

As shown in Figure 2, two thermal cameras and a servo hydraulic fatigue machine (MTS model 370) with a 100 kN loading capability were used for the experiments. In order to observe temperature stability, thermographic data was collected in a single sequence until the end of the test using a micro bolometric infrared camera FLIR A20 (160x140 pixels with a thermal sensitivity NETD $<$ 50 mK). Moreover, using the second camera, a cooled infrared camera X6540 with 640x512 pixels and a thermal sensitivity of NETD $<$ 20 mK, three thermographic sequences were obtained at a higher frame rate.

To remove the impact of ambient temperature on the mean surface temperature, a dummy-unloaded specimen composed of the same material was utilized as a temperature reference. To improve the surface roughness, the gage section was polished using sandpaper and moved through 480, 800, 1200, and 1500 grit sizes. Additionally, to increase the precision of the thermal signal, a matte black coating was added.

Table 2 Loading blocks for stepwise test

Loading block	1	2	3	4	5	6	7	8	9	10	11	12
% σ_u (MPa)	39.8	41.4	43	44.5	46.1	46.9	47.7	48.4	49.2	50	52.3	54.7
σ_a (MPa)	255	265	275	285	295	300	305	310	315	320	335	350

Fig. 2 Stepwise test setup

Thermographic acquisitions are carried out during the test utilizing an IR camera X6540 at 213 Hz for 10 seconds (2130 frames obtained) and a micro bolometric IR camera, FLIR A20, at 5 Hz for the same duration (50 frames acquired). Following a predetermined cycle count, the thermal sequence during each loading phase is recorded. Four sub-steps of thermal measurements were carried out for every loading phase, including 20,000 cycles. The data collected between 1000 and 1110 cycles, 5000 and 5110, 10000 -10110 cycles, and 15000-15110 cycles, respectively. The gauge length are between the extensometer's clips is considered as the region of interest (ROI).

The mean and harmonic components of a thermal signal can be obtained by processing acquired thermal data using a technique known as lock-in thermography [28]. The Fast Fourier Transform (FFT), which allows the temperature signal to be converted into its frequency-domain representation, requires a reference signal (load or strain) in order to process the temperature field. By modeling the temperature as follows, it is possible to obtain all of the temperature components [19]:

$$T(t) = T_0 + \Delta T f t + T_1 \sin(\omega t + \varphi_1) + T_2 \sin(\omega t + \varphi_2) \quad (1)$$

Where the temperature signal $T(t)$, f is the frequency of loading, T_0 is the temperature at the beginning, ΔT is the mean rise, T_1, φ_1, T_2, φ_2 are the amplitudes and phases of the 1st and 2nd Fourier components, respectively. Figure 3 (b) shows a schematic representation of thermal signal processing. As shown in Figure 3 (b), the chosen thermal indices in this work

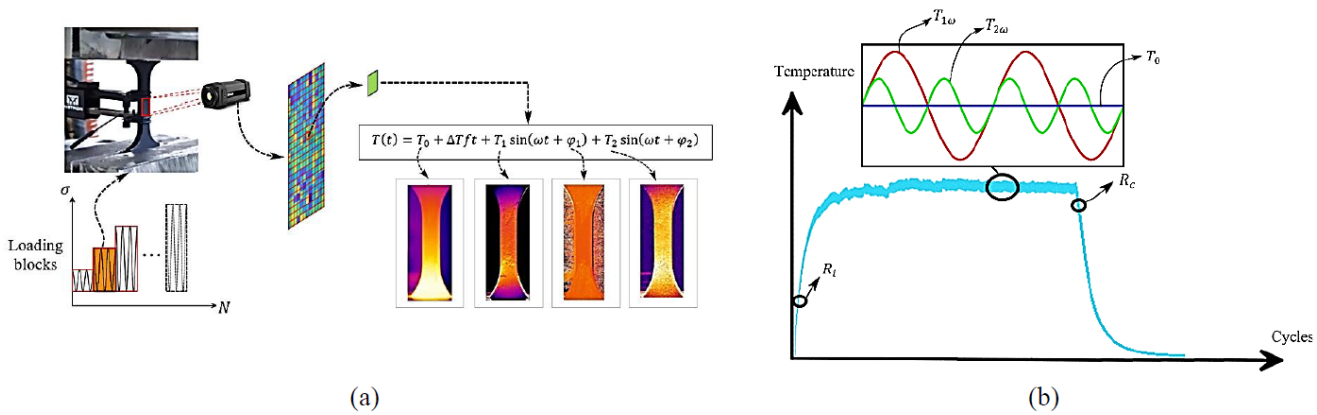

Fig. 3 (a) temperature components acquisition (b) a schematic representation of thermal indices

are: stabilized mean temperature (ΔT), initial slope of the mean temperature (R_i), first amplitude harmonic of temperature ($T_{1\omega}$), second amplitude harmonic of temperature ($T_{2\omega}$) and slope of the mean temperature in cooling stage (R_c).

A number of sequential procedures were engaged in the thermal data processing. First, $T(t)$ was obtained using an infrared thermal camera with a mm/pixel ratio of 0.116 mm. After that, IRTA® software was used to define a particular ROI, and temperature data over time was retrieved for further analysis. For every frame in the time sequence, the average temperature value ($T_0(t)$)) for this ROI was calculated. Next, Discrete Fourier Transform (DFT) was used to obtain harmonic components [29].

Results

The overall thermal behavior of samples at various loading levels is explained below. The average surface temperature change during the stepwise test obtained by the micro bolometric camera is shown in Figure 4. After each loading block, a cooling period of about a minute start after temperature stabilization and a specific number of cycles. After that, this process is repeated again until sample fails. Very high temperature, between 160 and 200 °C, was recorded at failure which can be due to the ductility of the material and work hardening.

The thermal footprint is shown for the 3^{rd} sample in Figure 5. Steps 1, 3, and 5 show a slight increase in temperature below the fatigue limit of 306 MPa [27], while steps 9 and 11 show a large increase, suggesting that damage accumulates until the specimen fails (step 11 is the step before the failure of the sample).

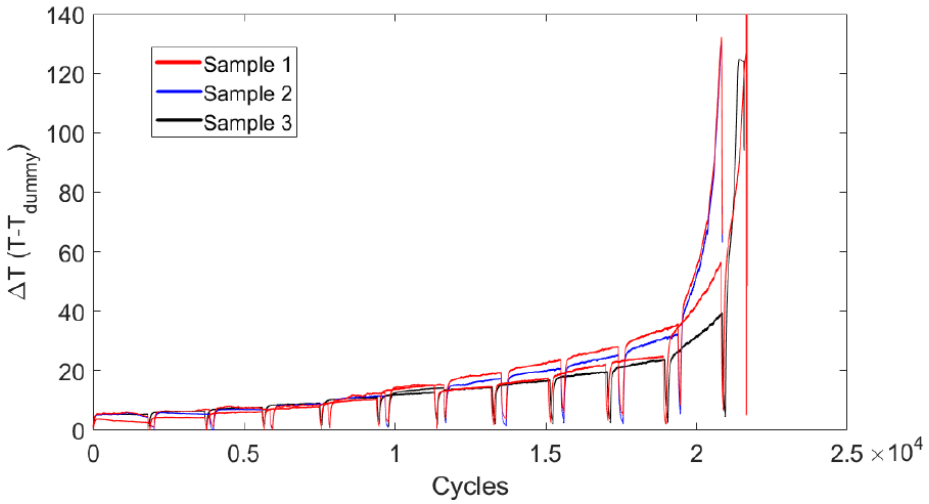

Fig. 4 Temperature trend obtained by a cooled camera for all samples

Figure 6 shows the trend of ΔT and R_c with stress level which was extracted using thermal data from the uncooled camera. ΔT was calculated by subtracting the mean surface temperature of the sample from that of the dummy sample. In the meantime, the gradient of the mean surface temperature during the cooling stage was calculated to determine R_c. Furthermore, the data obtained from the cooled camera was used for $T_{1\omega}$ and $T_{2\omega}$ since a higher sampling rate is required to reconstruct the temperature signal. Figure 7 provides these measured values.

Unlike the other indices, only for R_i, an analysis was conducted to check how the measurement of R_i can be influenced by sampling rate of thermal camera (cooled or uncooled camera) and the time period over which the fitting is applied to thermal data. Within time durations ranging from 1 to 10 seconds, linear fitting was used for the thermal points. It should be noted that the slope was determined using the data points where the temperature begins to climb and shows cyclic trend.

Figure 8 and Figure 9 propose the results only for sample 3 as an example. It is evident that curves from an uncooled camera show more obvious fluctuations, specifically for time duration of 1 to 3 seconds, that prevent the fatigue limit from being estimated from the datapoints, in contrast to curves found through fitting on the data from a cooled camera.

The trends from the cooled camera shows instability at 1 second but stabilizes for longer time duration, whereas for the uncooled camera, notable variations are clear for 1 to 2 seconds.

This analysis highlights the significance of taking precise measurements of the initial slope of the mean temperature. Therefore, it is recommended to use a cooled camera (or a large number of data points) instead of the uncooled one to have

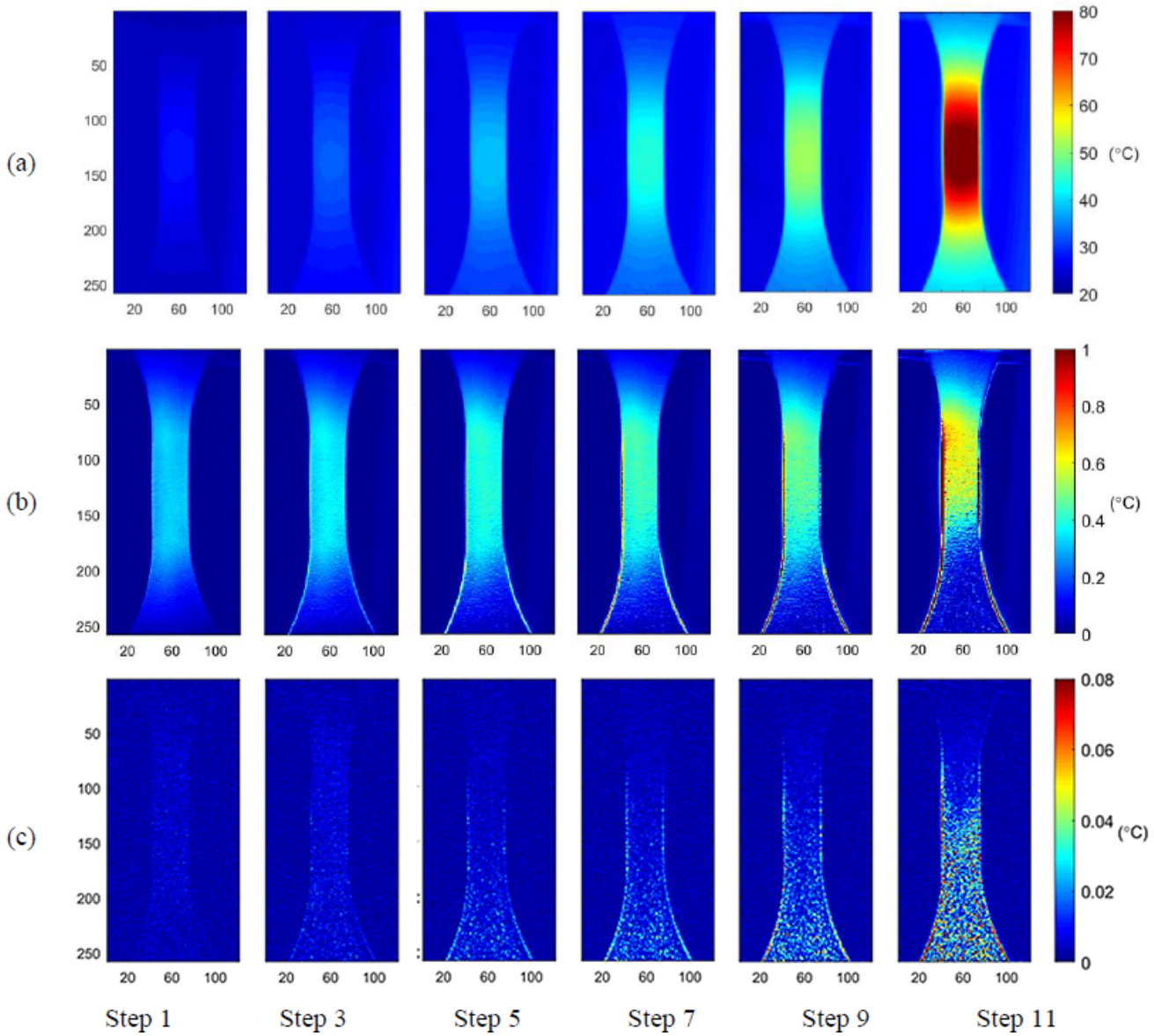

Fig. 5 Variation of thermal signature during stepwise test (sample 3): (a) ΔT (b) $T_{1\omega}$ (c) $T_{2\omega}$

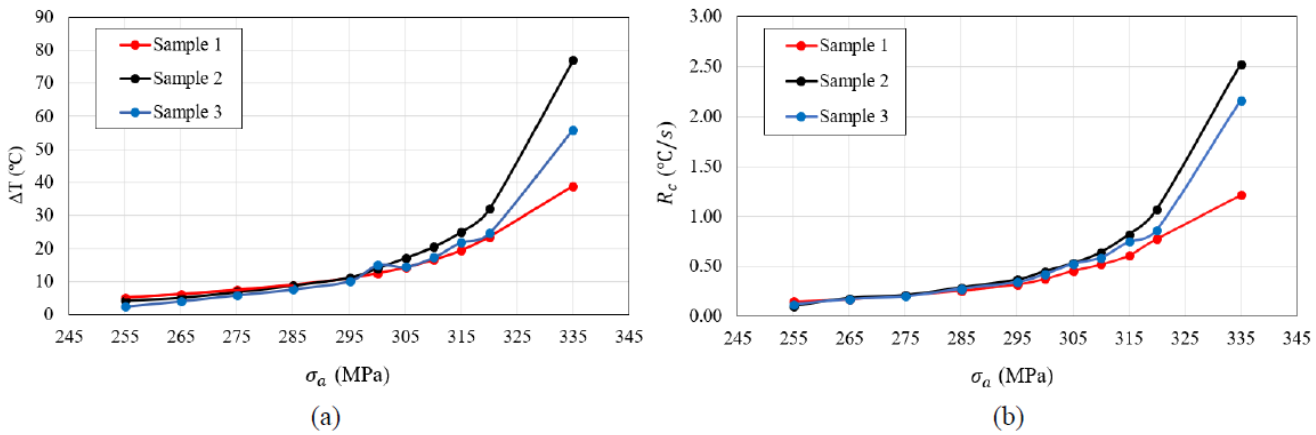

Fig. 6 (a) stabilized temperature rise, and (b) the slope of temperature during cooling stage

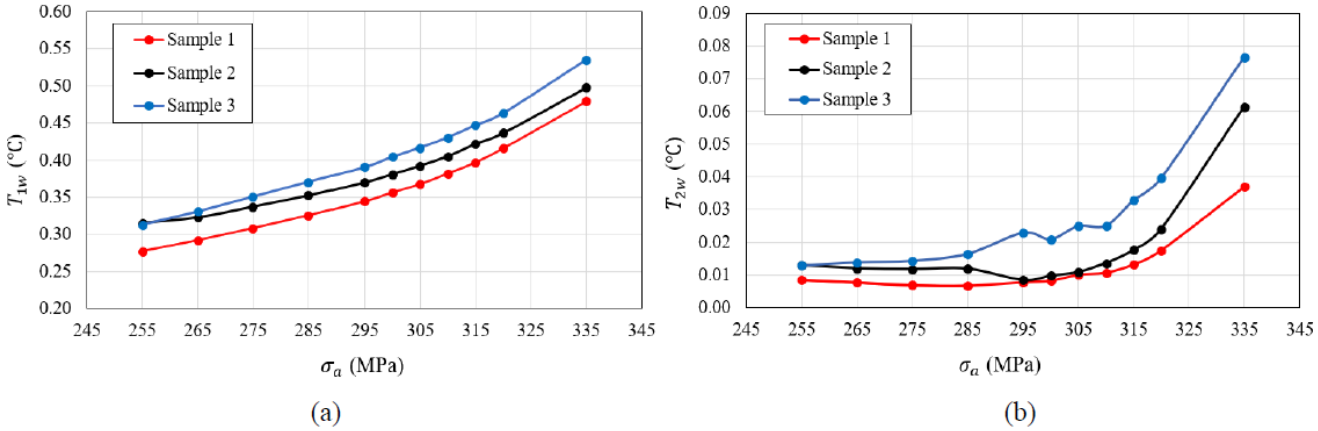

Fig. 7 (a) 1^{st} amplitude harmonic and (b) 2^{nd} amplitude harmonic of the temperature

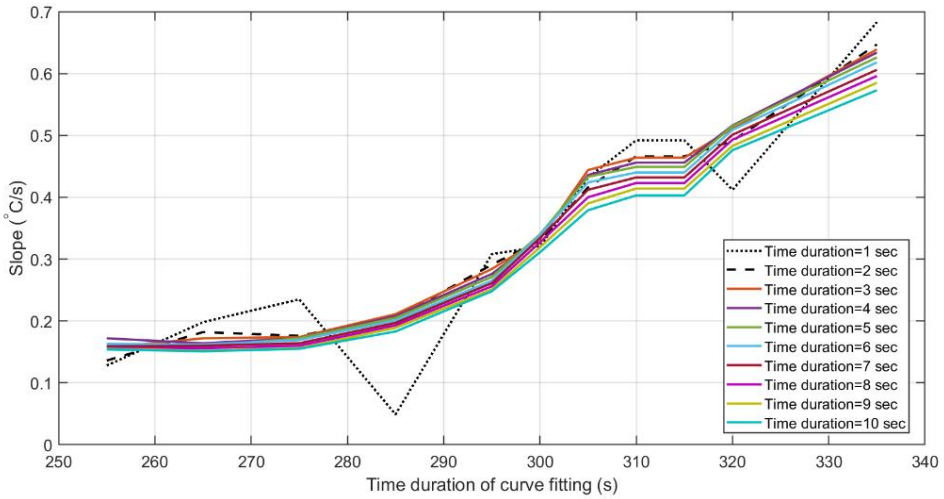

Fig. 8 Rising slope of temperature from linear fitting on uncooled camera data (sample 3)

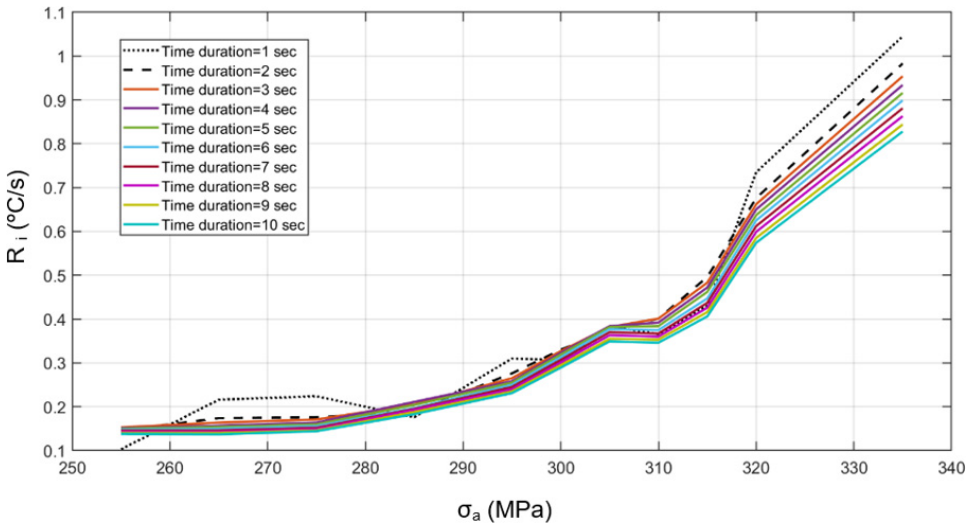

Fig. 9 Rising slope of temperature from linear fitting on cooled camera data (sample 3)

smoother trends. On the other hand, if an uncooled camera is the only choice, it is recommended that curve fitting be done for time durations longer than 2 seconds.

Furthermore, the accuracy of cooled and uncooled camera in fatigue limit prediction is presented below.

Not only for R_i but also for other indices studied here, Loung's method [30] was applied to estimate the fatigue limit.

It involves fitting two regression lines to data points in each thermal index trend that are clearly below and above the knee point [30]. The fatigue limit can be reliably approximated by finding the point where these two lines connect.

Unlike other indices which depends only on the stress level, R_i is also dependent on sampling rate as well as the time duration used for fitting. Thus, the fatigue limit predicted by R_i needs through investigation, as shown in Figure 10. The reference fatigue limit (derived from the S-N curve, 306 MPa [27]) is shown by the dashed red line. It is evident from the figure that, the predicted values from the cooled camera (yellow bars) are consistently closer to the reference value for durations of three seconds or more. Conversely, the estimated values for uncooled camera typically display lower predicted fatigue limits, which are farther away from the dashed line.

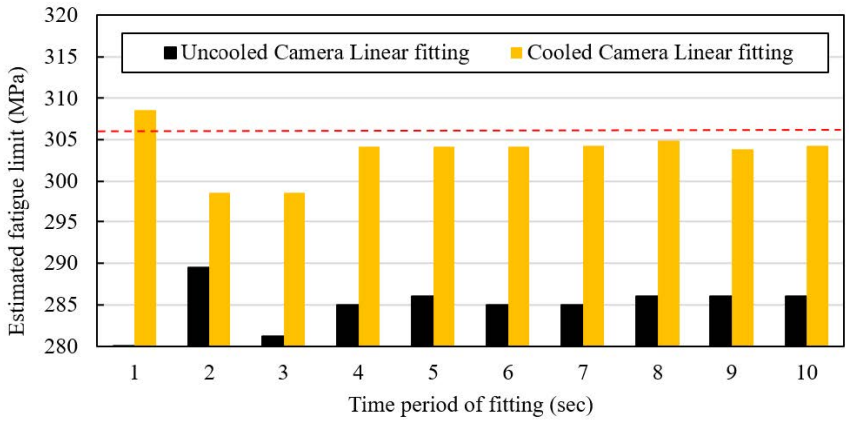

Fig. 10 Fatigue limit predicted by $\boldsymbol{R_i}$ (sample 3)

In light of this finding, the average of the predicted fatigue limits derived from all time periods was used to compare R_i with other thermal indices.

Table 3 shows the fatigue limit estimated using all considered thermal indices in this work. For each index, the discrepancy between the mean of the estimated values from 3 samples and the reference one is also included in the last column of Table 3.

According to the first column, $T_{2\omega}$ and R_i measured from the data acquired by a cooled camera show better performance and accuracy than the others, both showing only a 0.1% difference.

Estimation by ΔT ranks second with a difference of 1.6%. Other methods, such as $T_{1\omega}$, R_c, and R_i from uncooled camera, exhibit errors ranging from 2.1%, 2.9% and 4.4%, respectively.

Table 3 Predicted fatigue limit using Loung's method

Rank	Method	Predicted fatigue limit (MPa)				Difference* (%)
		Sample 1	Sample 2	Sample 3	Average	
1	$T_{2\omega}$(℃)	305.69	304.33	307.21	305.75	0.1
1	R_i (℃/s) from linear fitting and cooled camera	-	308.05	303.53	305.79	0.1
2	ΔT (℃)	303.35	300.00	300.00	301.12	1.6
3	$T_{1\omega}$(℃)	300.77	297.16	300.62	299.52	2.1
4	R_c (℃/s)	294.24	296.98	299.89	297.04	2.9
5	R_i (℃/s) from linear fitting and uncooled camera	296.02	296.34	285.52	292.62	4.4
*Difference with respect to the fatigue limit from S-N curve (306 MPa) [27]						

Conclusions

A thorough experimental campaign was carried out to examine the effectiveness of five thermal indices in fatigue limit prediction and determine the thermal response of SS 316 samples under cyclic loadings. The use of the same dataset is the strongest point of the comparison. For comparison, the difference between the reference fatigue limit value from the S-N curve and the estimated fatigue limit based on Loung's technique was evaluated.

From the results, $T_{2\omega}$ and R_i from cooled camera performed better than the other thermal indices studied, yielding the closest forecasts to the reference value, with 0.1% difference. ΔT, $T_{1\omega}$ and R_c show greater errors ranging from 1.6% to 2.9%. However, R_i from uncooled camera showed the worst performance, error of 4.4%.

As the main contribution of the work, the results emphasize how time duration for curve fitting and thermal acquisition techniques affect the precision of R_i fatigue limit prediction. The data obtained with a cooled camera yields the most accurate fatigue limit predictions, particularly when the fitting time is more than three seconds. On the other hand, estimations from an uncooled camera exhibit notable oscillation, which makes it difficult to make a reliable fatigue limit estimate. However, if an uncooled camera is the only option, it is recommended a fitting duration of at least 3 seconds for linear fitting to minimize error in fatigue limit estimation.

References

1. J. Schijve, Fatigue of Structures and Materials Springer Dordrecht, 2009.
2. S. Suresh, Fatigue of materials, Cambridge solid state science series, 1992.
3. F. Bjørheim, S.C. Siriwardane, D. Pavlou, A review of fatigue damage detection and measurement techniques, International Journal of Fatigue, 154 (2022) 106556.
4. R. Pippan, C. Zelger, E. Gach, C. Bichler, H. Weinhandl, On the mechanism of fatigue crack propagation in ductile metallic materials, Fatigue & Fracture of Engineering Materials & Structures, 34 (2011) 1-16.
5. G. Antaki, R. Gilada, Chapter 2 - Design Basis Loads and Qualification, in: G. Antaki, R. Gilada (Eds.) Nuclear Power Plant Safety and Mechanical Integrity, Butterworth-Heinemann, Boston, 2015, pp. 27-102.
6. S.M. Shepard, Advances in pulsed thermography, in: Advances in Pulsed Thermography. Proc. SPIE - The International Society for Optical Engineering, Thermosense XXVIII, Orlando, Florida, 2001.
7. C. Ibarra-Castanedo, N.P. Avdelidis, X.P. Maldague, Quantitative pulsed phase thermography applied to steel plates, in: Thermosense XXVII, International Society for Optics and Photonics, 2005.
8. G. Pitarresi, R. Cappello, A. Capraro, V. Pinto, D. Badagliacco, A. Valenza, Frequency modulated thermography-NDT of polymer composites by means of human-controlled heat modulation, in: P. Rizzo, A. Milazzo (Eds.) European Workshop on Structural Health Monitoring, Springer International Publishing, Cham, 2023, pp. 610-618.
9. E. D'Accardi, R. Krankenhagen, A. Ulbricht, M. Pelkner, R. Pohl, D. Palumbo, U. Galietti, Capability to detect and localize typical defects of laser powder bed fusion (L-PBF) process: an experimental investigation with different non-destructive techniques, Progress in Additive Manufacturing, 7 (2022) 1239-1256.
10. G. Dell'Avvocato, D. Gohlke, D. Palumbo, R. Krankenhagen, U. Galietti, Quantitative evaluation of the welded area in resistance projection welded (RPW) thin joints by pulsed laser thermography, SPIE, 2022.
11. N. Montinaro, D. Cerniglia, G. Pitarresi, Evaluation of vertical fatigue cracks by means of flying laser thermography, Journal of Nondestructive Evaluation, 38 (2019) 48.
12. D. Palumbo, R. De Finis, U. Galietti, Thermoelastic stress analysis as a method for the quantitative non-destructive evaluation of bonded CFRP T-joints, NDT & E International, 124 (2021) 102526.
13. M. Zaeimi, R. De Finis, D. Palumbo, U. Galietti, Fatigue limit estimation of metals based on the thermographic methods: A comprehensive review, Fatigue & Fracture of Engineering Materials & Structures, 47 (2024) 611-646.
14. M. Zaeimi, R. De Finis, D. Palumbo, U. Galietti, Numerical Simulation of the Heat Dissipation During the Fatigue Test, in: C. Franck, K. Kasza, J. Estrada, R. De Finis, G. Ólafsson, S. Gururaja, J. Furmanski, A. Forster, P. Kolluru, M. Prime, T. Berfield, C. Aydiner (Eds.) Challenges in Mechanics of Biological Systems and Materials, Thermomechanics and Infrared Imaging, Time Dependent Materials and Residual Stress, Volume 2, Springer Nature Switzerland, Cham, 2024, pp. 83-90.
15. M. Zaeimi, R. De Finis, D. Palumbo, U. Galietti, A Hybrid Approach for Heat Source Identification and Heat Diffusion–Related Issues in the Fatigue Loading, Fatigue & Fracture of Engineering Materials & Structures, n/a (2025).
16. G. La Rosa, A. Risitano, Thermographic methodology for rapid determination of the fatigue limit of materials and mechanical components, International Journal of Fatigue, 22 (2000) 65-73.
17. M. Mehdizadeh, M.M. Khonsari, On the application of fracture fatigue entropy to variable frequency and loading amplitude, Theoretical and Applied Fracture Mechanics, 98 (2018) 30-37.
18. D. Palumbo, U. Galietti, Thermoelastic Phase Analysis (TPA): a new method for fatigue behaviour analysis of steels, Fatigue & Fracture of Engineering Materials & Structures, 40 (2017) 523-534.
19. J.C. Krapez, D. Pacou, G. Gardette, Lock-in thermography and fatigue limit of metals, in: 2000 Quantitative InfraRed Thermography, 2000.
20. R. De Finis, D. Palumbo, U. Galietti, On the relationship between mechanical energy rate and heat dissipated rate during fatigue for a C45 steel depending on stress ratio, Fatigue & Fracture of Engineering Materials & Structures, 44 (2021) 2781-2799.

21. R.D. Finis, D. Palumbo, A. Pirinu, A. Saponaro, F.W. Panella, R. Nobile, U. Galietti, Fatigue behaviour assessment of C45 steel by means of energy-based methods, in: IOP Conference Series: Materials Science and Engineering, 2021.
22. G. Meneghetti, Analysis of the fatigue strength of a stainless steel based on the energy dissipation, International Journal of Fatigue, 29 (2007) 81-94.
23. M. Naderi, M. Amiri, M.M. Khonsari, On the thermodynamic entropy of fatigue fracture, Proceedings of the Royal Society A: Mathematical, Physical and Engineering Sciences, 466 (2010) 423-438.
24. A. Risitano, G. Risitano, Determining fatigue limits with thermal analysis of static traction tests, Fatigue & Fracture of Engineering Materials & Structures, 36 (2013) 631-639.
25. C. Colombo, L. Vergani, Thermographic applications for the rapid estimation of fatigue limit, Procedia Structural Integrity, 24 (2019) 658-666.
26. M. Ricotta, G. Meneghetti, B. Atzori, G. Risitano, A. Risitano, Comparison of experimental thermal methods for the fatigue limit evaluation of a stainless steel, Metals, 9 (2019) 677.
27. A. Mahmoudi, M.M. Khonsari, A Thermodynamic Framework for Rapid Prediction of S-N Curves Using Temperature Rise at Steady-State, Experimental Mechanics, (2023).
28. C. Colombo, M. Sansone, L. Patriarca, L. Vergani, Rapid estimation of fatigue limit for C45 steel by thermography and digital image correlation, The Journal of Strain Analysis for Engineering Design, 56 (2021) 478-491.
29. A. Aghayan, P. Jaiswal, H.R. Siahkoohi, Seismic denoising using the redundant lifting scheme, GEOPHYSICS, 81 (2016) V249-V260.
30. M.P. Luong, Fatigue limit evaluation of metals using an infrared thermographic technique, Mechanics of Materials, 28 (1998) 155-163.